Journal of Materials Chemistry A

PAPER

View Article Online
View Journal | View Issue

Check for updates

Cite this: J. Mater. Chem. A, 2019, 7, 26116

Ultra-stable $CsPbBr_3$ nanocrystals with near-unity photoluminescence quantum yield *via* postsynthetic surface engineering†

Yanqing Zu,[a] Jinfei Dai,[a] Lu Li,[a] Fang Yuan,[a] Xiang Chen,[b] Zhicun Feng,[b] Kun Li,[a] Xiaojuan Song,[a] Feng Yun,[a] Yue Yu,[a] Bo Jiao,[a] Hua Dong,[a] Xun Hou,[a] Minggang Ju *[c] and Zhaoxin Wu *[ad]

Received 2nd August 2019
Accepted 15th October 2019

DOI: 10.1039/c9ta08421e

rsc.li/materials-a

Lead halide perovskite nanocrystals (NCs) have recently attracted intense interest as promising luminophores for optoelectronic devices. However, their extensive applications are still hampered by a high-cost synthesis method and the poor stability and low photoluminescence quantum yield (PLQY) of NCs. To address these issues, herein, a fast, room-temperature method is adopted to prepare $CsPbBr_3$ NCs with the use of green synthetic solvents. More importantly, we explore an efficient postsynthetic dual-surface-passivation strategy of $CsPbBr_3$ NCs with 1,3-adamantanedicarboxylic acid (ADA) and $ZnBr_2$ ligands, which exhibits near-unity PLQY and ultra-high stability. The theoretical results show that such a remarkable performance stems from efficient passivation of the massive surface defects of $CsPbBr_3$ with ADA and $ZnBr_2$, suppressing the formation of surface nonradiative recombination centers. Besides, we fabricated white light-emitting diodes (WLEDs) based on essentially trap-free $CsPbBr_3$ NCs. The optimal device exhibits a luminous efficiency of up to 68.7 lm W^{-1} and wide color gamut of 119% of the NTSC standard.

Introduction

All-inorganic $CsPbX_3$ (X = Br, Cl, I) colloidal nanocrystals (NCs) have recently demonstrated unprecedented progress for various optoelectronic devices, such as lasers, photodetectors, photovoltaic devices and light-emitting diodes (LEDs).[1–5] In particular, they are promising candidates for high-definition displays, due to their low cost, excellent thermal stability and narrow bandwidths (about 20 nm).[6–9] However, they have not yet been realized for commercial applications, which are typically hindered by (a) a tedious and high-expense preparation method; (b) the poor stability and low photoluminescence quantum yield (PLQY). There is still an urgent need to solve these problems.

A hot-injection method is commonly used to synthesize perovskite NCs, which needs to be performed at high temperature and an inert atmosphere. This tedious approach unavoidably increases the cost and limits the output.[8,10] Therefore, the synthesis of NCs at room temperature in air is highly desired for low-cost and large-scale preparation.[11,12] During isolation and purification of NCs, because the ligands possess a high diffusion coefficient in solution up to 166 μm^2 s^{-1}, they easily desorb from the NC surface,[13–19] leading to various defects. For example, a lead-rich surface creates deep defect levels ($>5k_bT$), whereas the halogen-deficient surface produces vacancies as the major defect type that introduces shallow ($<5k_bT$) defect levels. These defects will weaken the photoluminescence of NCs.[20–26,29] The postsynthetic defect passivation has been considered as an effective strategy to tackle this issue *via* introducing a range of ligands, that is, Lewis bases, including inorganic salts (NH_4SCN and $NaBF_4$),[27,28] organic molecules (hexylphosphonic acid and 2,2′-iminodibenzoic acid)[29,30] and inorganic–organic hybrids (decyldimethylammonium bromide and its sulfide).[31,32] The above ligands have been used for passivation of the high-temperature synthesized NCs, whose surface chemistry is different from NCs prepared at room temperature. To the best of our knowledge, there are rare ligands available for passivation of the room-temperature synthesized NCs.

In this work, a rapid, room-temperature method is adopted for the synthesis of $CsPbBr_3$ NCs. More importantly, 1,3-adamantanedicarboxylic acid (ADA) and $ZnBr_2$ ligands are rationally designed to passivate the surface traps, and density

[a]Department of Electronic Science and Technology, School of Electronic and Information Engineering, Xi'an Jiaotong University, Xi'an 710049, Shaanxi, People's Republic of China. E-mail: zhaoxinwu@mail.xjtu.edu.cn

[b]School of Chemical Engineering, Northwest University, Xi'an 710069, Shaanxi, People's Republic of China

[c]Department of Chemistry, University of Nebraska-Lincoln, Lincoln, Nebraska, 68588, USA. E-mail: juming@mail.ustc.edu.cn

[d]Collaborative Innovation Center of Extreme Optics, Shanxi University, Taiyuan 030006, People's Republic of China

† Electronic supplementary information (ESI) available. See DOI: 10.1039/c9ta08421e

functional theory (DFT) calculations are used to unveil their roles in affecting the optical properties of $CsPbBr_3$ NCs. This dual-surface passivation renders the PLQY of $CsPbBr_3$ NCs close to unity (97.1%) and durable stability (a 7% decrease in PLQY after 65 days). Our theoretical results show that these ligands can effectively passivate the surface defects of $CsPbBr_3$ NCs and suppress the formation of surface nonradiative recombination centers. In addition, a white light-emitting diode (WLED) device was also successfully fabricated with green-emissive $CsPbBr_3$, red emitting K_2SiF_6:Mn^{4+} phosphor on a blue emitting GaN chip and exhibits a high luminous efficiency of 68.7 lm W^{-1} and wide color gamut of 119% of the NTSC standard, indicating a great application potential for backlight displays.

Results and discussion

Theoretical calculation

Density functional theory (DFT) calculation was used to predict the passivation role of ADA and $ZnBr_2$ in the halide-deficient surfaces of $CsPbBr_3$. Note that the band gap of $CsPbBr_3$ is generally underestimated using the PBE functional with spin-orbital coupling (SOC), resulting in inaccurate estimation for defect states of $CsPbBr_3$. To overcome this issue, the PBE0 functional with SOC is adopted in our study and has been verified to accurately characterize lead halide perovskite in previous work.[33] It is well known that pristine $CsPbBr_3$ crystals terminated by CsBr facets exhibit a fully delocalized, trap-free band structure and differences in the electronic structure between pristine and halide-deficient surfaces can be directly attributed to surface halide vacancies. Herein, two different defects are considered, V_{Br} and V_{2Br}, in which there exist one and two Br vacancies on the surface, respectively. From Fig. S1a and 1b,† it is obvious that the defect states V_{Br} and V_{2Br} lead to the formation of trap states in the band gap, highly localized on the top surface layer, which acts as an electron-trapping center. In addition, the VBM and CBM are fully delocalized on the structure of $CsPbBr_3$. After passivation of ADA, fully delocalized VBM and CBM states with trap-free band gaps were observed for $CsPbBr_3$, indicating that ADA can effectively alter the energetics of Br vacancy defects of $CsPbBr_3$, removing them from the band gaps (Fig. 1a and b). Moreover, Pb–Br ion pair defects are unavoidably formed on the surface of $CsPbBr_3$ due to non-passivated sites. To gain insight into the mechanism of surface treatment using $ZnBr_2$, similar with previous studies,[34] three models are considered (Fig. 1c and S2†): (a) an ideal $CsPbBr_3$ surface, (b) with a removed Pb–Br ion pair on the surface, and (c) treatment with a filled Zn–Br ion pair at the surface. It can be seen that the Pb–Br ion pair defect leads to a trap state on the VBM that is localized on the top surface layer. After surface treatment with $ZnBr_2$, the VBM is fully delocalized on the $CsPbBr_3$, demonstrating that $ZnBr_2$ can effectively passivate the Pb vacancy defect. Interestingly, through the surface treatment with ADA and $ZnBr_2$, the Br and Pb vacancy defects are passivated, resulting in the PL enhancement of $CsPbBr_3$. Lastly, we rationally proposed the dual-passivation mechanism for $CsPbBr_3$ NCs, as shown in Fig. 1d.

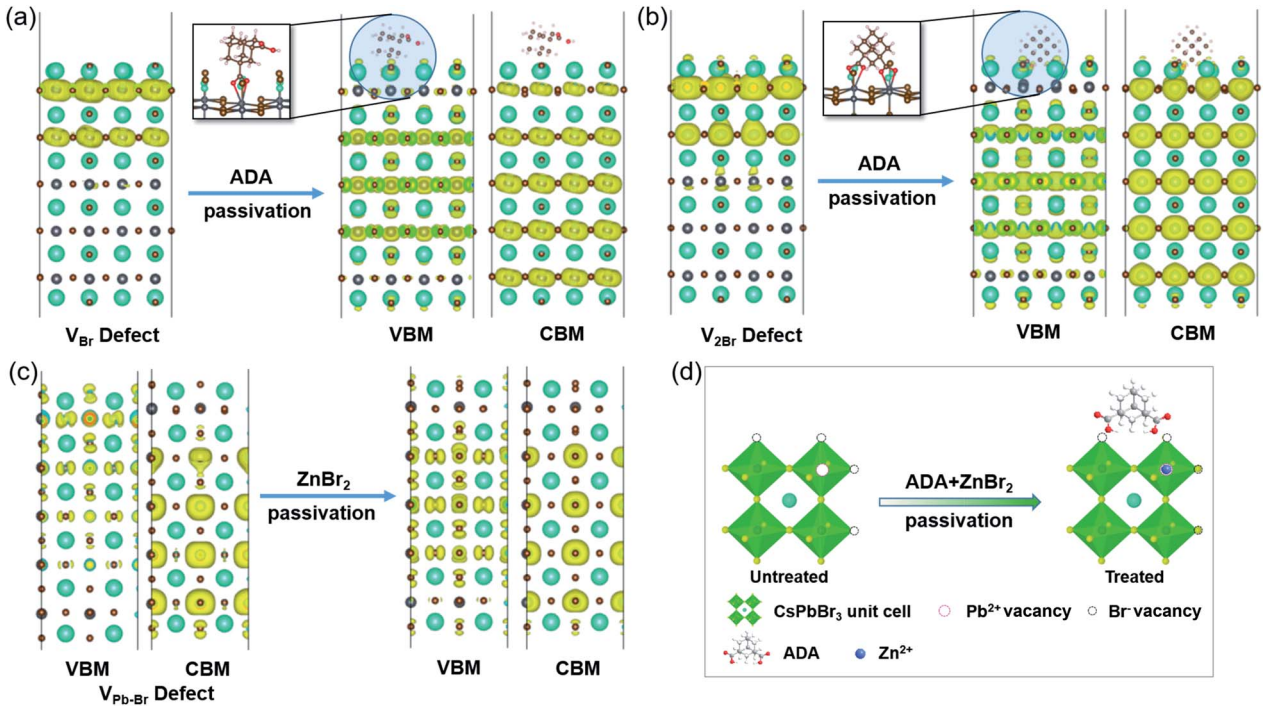

Fig. 1 Charge density calculations at the PBE0+SOC level of theory for (a) $CsPbBr_3$ with a surface Br vacancy ($CsPbBr_3$ + V_{Br}) without and with ADA passivation. (b) $CsPbBr_3$ with two surface Br vacancies ($CsPbBr_3$ + $2V_{Br}$) without and with ADA passivation. (c) Electronic charge density for the VBM and CBM for $CsPbBr_3$ with a surface Pb–Br vacancy ($CsPbBr_3$ + V_{Pb-Br}) without and with $ZnBr_2$ passivation. Cs, Pb and Br atoms are shown as blue-green, gray and purple, respectively. (d) Schematic illustration of the proposed sequential passivation mechanism for $CsPbBr_3$ NCs.

Synthesis and characterization

Colloidal $CsPbBr_3$ NCs were prepared by a modified ligand-assisted reprecipitation method,[10] and propionic acid (PAD) and oleylamine (OLAm) were used as surface capping ligands. In a typical synthesis, the Cs_2CO_3 and $PbBr_2$ precursors were obtained separately. First, the Cs_2CO_3 precursor was injected into the mixed solvent of hexane and isopropanol under vigorous stirring to form a colorless solution. Second, the $PbBr_2$ precursor was rapidly injected into the above solution, and the colorless solution immediately turns green and then yellow, as shown in Fig. S3a†. Ten seconds later, the precipitate was separated from the solution through centrifugation and then redispersed into hexane (see the ESI† for further details). Furthermore, the dual surface passivation process was briefly described as follows: the ADA ligands were added to $CsPbBr_3$ NC hexane solution, following by an ultra-slow stirring and then high speed centrifugation. Subsequently, $ZnBr_2$ hexane solution was added, followed by an ultra-slow stirring (Fig. S3b) (see the ESI† for further details). To study the variation on the morphology of NCs with the dual-surface passivation, transmission electron microscopy (TEM) measurements were performed to gain insight into the microstructure of NCs with and without treatment. TEM images (Fig. 2a–c) and size distribution histograms (insets in Fig. 2a–c) show that the untreated, ADA-treated and (ADA + $ZnBr_2$)-treated samples all possess cube shaped morphologies with average diameters of 13.3 ± 2.4, 13.2 ± 2.7 and 13.7 ± 2.9 nm, respectively. Notably, there exist the "black dots" on the surface of the untreated NCs, which have been demonstrated as the decomposed products of the untreated $CsPbBr_3$ NCs under electron beam continuous irradiation, that is, $PbBr_2$, not the Pb^0 in previous studies. High-resolution transmission electron microscopy (HRTEM) images show that the three samples have the same lattice distance of

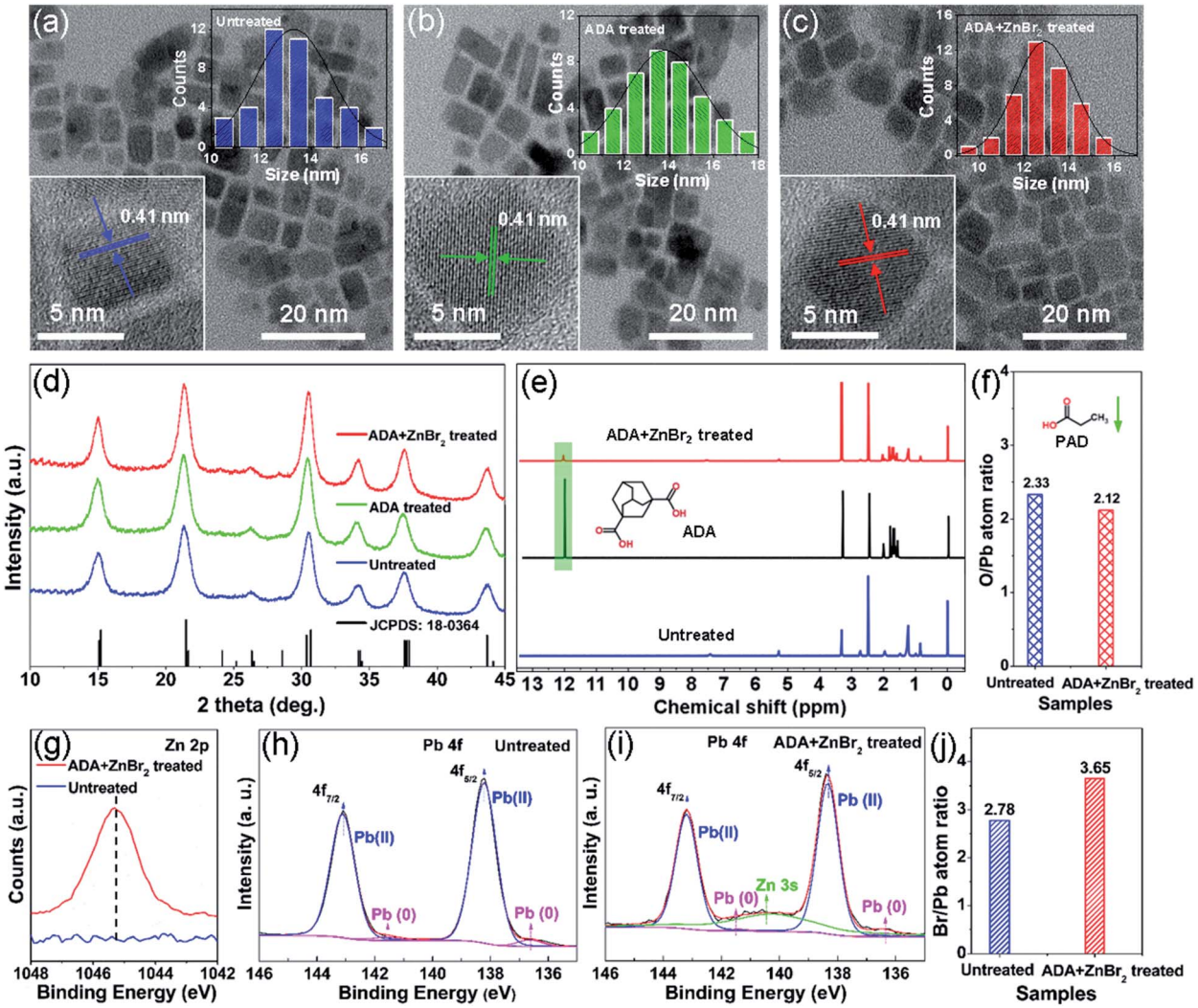

Fig. 2 TEM images of (a) untreated NCs, (b) ADA-treated NCs, (c) (ADA + $ZnBr_2$) treated NCs. The insets in (a)–(c) show the size distribution histograms and HRTEM images for the above corresponding NCs. (d) XRD patterns of untreated NCs, ADA-treated NCs and (ADA + $ZnBr_2$)-treated NCs. (e) ^1H NMR spectra of untreated NCs, pure ADA, and (ADA + $ZnBr_2$)-treated NCs. (f) Statistical O/Pb atomic ratios for untreated and ADA + $ZnBr_2$ treated samples calculated from XPS data. XPS spectra of (g) Zn 2p and (h) and (i) Pb 4f for both untreated and ADA + $ZnBr_2$ treated samples, respectively. (j) Statistical Br/Pb atomic ratios for untreated and ADA + $ZnBr_2$ treated NCs calculated from XPS data.

0.41 nm (insets in Fig. 2a–c), corresponding to the (110) crystal plane of the orthorhombic phase perovskite, thereby indicating that the crystal structure remains unchanged during post-treatment, also further confirmed by the X-ray diffraction (XRD) results (Fig. 2d). In addition, proton nuclear magnetic resonance spectroscopy (^{1}H NMR) and X-ray photoelectron spectroscopy (XPS) were also employed to investigate the organic–inorganic materials (ADA and $ZnBr_2$) absorbed on NC surfaces. The ^{1}H NMR spectrum of pure ADA shows the characteristic resonance at 12.16 ppm that is a signal of two carboxylic groups, while this signal in (ADA + $ZnBr_2$)-treated NCs also appeared at 12.14 ppm with the severely weakened intensity (Fig. 2e), suggesting that –COOH functional groups of ADA have been protonated, and ADA was tightly absorbed on the NC surfaces *via* hydrogen bonding.[30,35,36] Moreover, the other resonances of ADA are also present in (ADA + $ZnBr_2$)-treated samples. Obtained from the XPS results, the O and Pb atom ratio slightly decreases after the ADA + $ZnBr_2$ treatment, suggesting that the organic PAD was partly replaced by them (Fig. 2f). Inorganic $ZnBr_2$ has been used for *in situ* passivation of $CsPbBr_3$ NCs in early studies.[24] It should be noted that the XRD results demonstrated the formation of the $CsPbBr_3$ perovskite structure and the absence of discernible Zn-related impurity peaks in $ZnBr_2$–$CsPbBr_3$ NCs. Besides, XPS analysis further verified the absence of Zn ions on the surface of $ZnBr_2$–$CsPbBr_3$ NCs. Afterwards, $ZnBr_2$ and tetraoctylammonium bromide (TOAB) were used for post-synthetic treatment of $CsPbBr_3$ NCs.[37] The results showed that Zn^{2+} was not incorporated into the perovskite lattice possibly due to the smaller bond dissociation energy of Zn–Br (138 kJ mol^{-1}) in comparison with Pb–Br (314 kJ mol^{-1}). However, the XPS results indicated the existence of Zn^{2+} on the NC surface. Our XPS results confirmed the appearance of Zn 2p peaks on the NC surface and showed that the Zn^{2+} could passivate the under-coordinated Pb vacancy defects. As for the untreated NCs, there appears to be two intense peaks at 138.2 eV ($4f_{7/2}$) and 143.1 eV ($4f_{5/2}$), which correspond to lead ions. In addition, two weak peaks are attributed to Pb^0 because the formation of Pb^0 becomes inevitable during the synthesis of NCs. After the NCs are treated with ADA + $ZnBr_2$, the Pb 4f XPS spectra shifts to a higher binding energy of about 0.1 eV for (ADA + $ZnBr_2$)-treated samples in comparison with untreated NCs, indicating an improvement of Pb–Br species in NCs, evidently visualized by the peak fitting (Fig. 2h and i). Moreover, quantitative XPS analysis indicates a Br/Pb ratio of 2.78/1 for the untreated NC surface, whereas this ratio is improved to 3.65/1 after ADA + $ZnBr_2$ treatment, resulting in the bromide-rich surface (Fig. 2j).

Optical performance and stability

Fig. 3a shows the UV-vis absorption and PL spectra of untreated NCs, ADA-treated NCs and (ADA + $ZnBr_2$)-treated NC colloidal solution. It can be seen that the ADA-treated $CsPbBr_3$ NCs exhibit an obvious improvement of PL emission (PLQY from 39.6% to 55.2%), while the treatment with $ZnBr_2$ could enhance

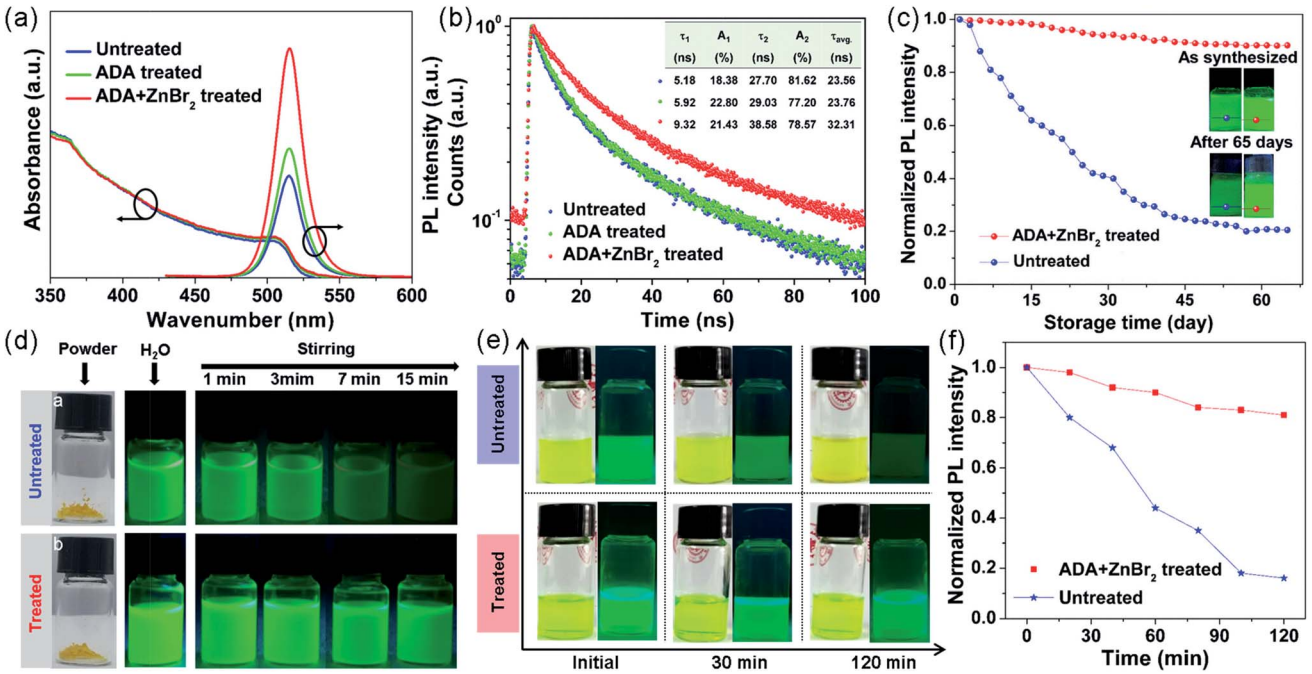

Fig. 3 (a) UV-vis absorption and PL spectra of $CsPbBr_3$ NCs before and after treatment. (b) Time resolved photoluminescence lifetimes (TRPLs) for NCs before and after treatment. The TRPL decay curves were fitted with a biexponential decay function, where A and τ refer to the amplitude components and lifetimes, respectively. The inset table shows the average lifetime ($\tau_{ave.}$), which is defined as $\tau_{ave.} = A_1\tau_1 + A_2\tau_2$. (c) Normalized PL intensity of samples before and after treatment aged for 65 days and the inset showing the corresponding colloid solutions under UV light. (d) Photographs displaying the stability against water for untreated and (ADA + $ZnBr_2$)-treated NCs, when stirred for 15 min. (e) Photographs of untreated and (ADA + $ZnBr_2$)-treated NC solution before and after thermal treatment at 80 °C for 2 h under daylight and UV light. (f) The normalized PL intensity of untreated and (ADA + $ZnBr_2$)-treated NCs before and after thermal treatment at 80 °C for 2 h.

the PL intensity with a 2-fold increase (PLQY from 39.6% to 79.5%), which is superior to that of $PbBr_2$ treatment (Fig. S4 and S5†). Surprisingly, when the samples were sequentially modified with ADA and $ZnBr_2$, there is nearly 2.5-fold enhancement of the PL intensity (PLQY ~ 97.1%) with respect to untreated NCs. Notably, the addition order of ADA and $ZnBr_2$ for post-synthetic NC treatment has no obvious effect on the PLQY (Fig. S6†), and the sequential passivation treatment with ADA and $ZnBr_2$ is slightly better than their simultaneous treatment (Fig. S7 and S8†), possibly due to the coordination competition of ADA with Pb^{2+} ions or Zn^{2+} ions. Considering the significant enhancement on the PLQY of samples with ADA/$ZnBr_2$ sequential treatment, there is an accompanying change on the PL lifetime. Through time-resolved photoluminescence (TRPL) measurements, it can be seen that a huge increase in the average PL lifetime (τ_2 from 27.70 to 38.58 ns) and long radiative lifetime is observed after post-treatment (Fig. 3b and its inset). The origin of enhancement of the PLQY along with prolongation of the PL lifetime of treated NC samples is ascribed to sequential passivation of surface defect states *via* (a) the strong coordination between two carboxyl groups of ADA and under-coordinated surface Pb atoms and (b) the surface Pb–Br ion pair defect passivation by Zn^{2+} and Br^- ions. In order to verify whether the dual-surface passivation could improve the colloidal stability or not, their time and moisture-dependent photostability tests were performed. The PLQY of (ADA + $ZnBr_2$)-treated NCs has a slight reduction of about 7% even after aging for 65 days. In contrast, the PLQY of untreated NCs rapidly drops from 39.6% to 19.1% (Fig. 3c). It is further demonstrated from the photographs that $CsPbBr_3$ NC solution with the dual-passivation shows a much better stability than NCs without treatment under 365 nm UV light (inset in Fig. 3c). Moreover, when different NC powders were immersed in water as an extreme situation, the (ADA + $ZnBr_2$)-treated NCs show a stronger brightness under UV light (365 nm) (Fig. 3d) and a less reduction in PL intensity (Fig. S9†), demonstrating that not only shallow and deep traps of the NC surface are essentially removed with (ADA + $ZnBr_2$) treatment, but also the ultra-large steric hindrance of ADA blocks the attack of water molecules and ensures the stability of NCs. After being annealed at 80 °C for 120 min, the ADA + $ZnBr_2$ treated NC colloids enable a great dispersion to be maintained. However, the untreated NC colloidal solution turned cloudy because the NC sizes tend to increase and aggregate apparently (Fig. 3e). Besides, the ADA + $ZnBr_2$ treated NCs showed brighter luminescence than untreated NCs under 365 nm UV light. Accordingly, the PL intensity of ADA + $ZnBr_2$ treated NCs maintained at 80% of the initial value, and the PL peak wavenumber was only redshifted from 515 to 516 nm. Nevertheless, the PL intensity of the untreated NCs decreased significantly, and an obvious red shift from 515 to 520 nm of PL emission can be observed (Fig. S10†). The TEM images further demonstrate that there is no obvious change in the size of ADA + $ZnBr_2$ treated NCs whereas the untreated NCs exhibited a serious agglomeration (Fig. S11†). In a word, the PLQY and stability of passivated $CsPbBr_3$ NCs were comparable to or even better than those of state-of-the-art pervoskite NCs (Table S1†).

Backlight displays

Large-scale passivated $CsPbBr_3$ NC inks are readily achieved without notable shape variation (Fig. 4a and S12†). We have also designed white light-emitting diode (WLED) devices that are constructed using passivated $CsPbBr_3$ green emitters and red emissive phosphor K_2SiF_6:Mn^{4+} on a blue emissive GaN chip. Fig. 4b shows the electroluminescence (EL) spectrum of WLEDs, and there exist three EL peaks (460 nm of the blue GaN chip, 515 nm of $CsPbBr_3$ NCs and 630 nm of K_2SiF_6:Mn^{4+}), corresponding to the CIE coordinate of (0.16, 0.03), (0.11, 0.76) and (0.69, 0.31), respectively. As shown in Fig. 4c, the CIE coordinate of ADA + $ZnBr_2$ treated NCs is obtained and compared with the advanced green-emitting materials such as $CsPbBr_3$ NCs,[38] $MAPbBr_3$,[39] Cd-based quantum dots,[40] $Ba_3Si_6O_{12}N_2$:Eu[41] and α-sialon:Yb^{2+},[42] which might contribute to an even wider color gamut of the WLEDs. The optimized WLEDs exhibit a color rendering index of (CRI) of 74 and a luminous efficiency of 68.7 lm W^{-1} (higher than those of an incandescent lamp of 17.0 lm W^{-1}) and wide color gamut (~119% of the National Television Standard Committee (NTSC) standard) at an operating voltage of 2.6 V. The CIE chromaticity coordinate of the WLEDs is (0.33, 0.31), as displayed in Fig. 4d, very close to standard white emission (0.33, 0.33), which provides the possibility for backlight display application.

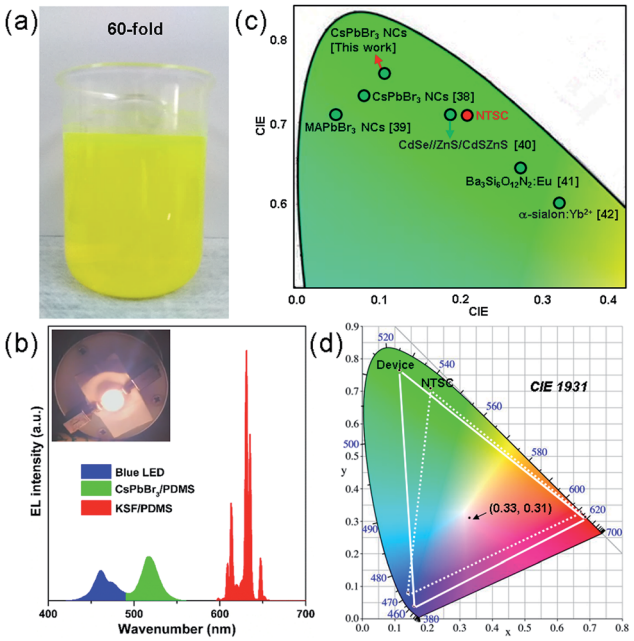

Fig. 4 (a) Photograph of scaled-up 60-folds of ADA + $ZnBr_2$ passivated $CsPbBr_3$ NC solution. (b) The color coordinates of ADA + $ZnBr_2$ treated $CsPbBr_3$ NCs on the CIE 1931 color space compared with other green-emitting materials, including $CsPbBr_3$ NCs, $MAPbBr_3$, Cd-based quantum dots, $Ba_3Si_6O_{12}N_2$:Eu and α-sialon:Yb^{2+}. (c) Electroluminescence (EL) spectra of white light-emitting diodes (WLEDs) assembled by covering the above green-emitting $CsPbBr_3$ and red-emitting K_2SiF_6:Mn^{4+} film on a blue-emitting GaN chip. (d) The color coordinate of the constructed WLEDs is shown in the CIE 1931 diagram.

Conclusions

In conclusion, we adopt a rapid, room-temperature synthesis of $CsPbBr_3$ NCs, and ADA + $ZnBr_2$ ligands are used to passivate the NC surface traps. These passivated NCs exhibit the near-unit PLQY and robust colloidal stability. Our theoretical results also provide an insightful understanding of the effective passivating roles that these ligands are capable of eliminating the vacancy defects and suppressing the formation of surface nonradiative recombination centers. Finally, we fabricated WLEDs based on essentially defect-free $CsPbBr_3$ NCs, showing a bright future in the field of display technology. As a result, this dual-surface-passivation strategy might pave the universal way for achieving high-quality NCs that can be widely used in various optoelectronic devices.

Conflicts of interest

There are no conflicts to declare.

Acknowledgements

This work was financially supported by the National Natural Science Foundation of China (Grant No. 11574248), the National Key R&D Program of China (Grant No. 2016YFB0400702), and the National Natural Science Foundation of China (Grant No. 61505161). We expressed our gratitude for the help that Dr X. J. Zhang and Dr J. J. Zhang from the School of Science of Xi'an Jiaotong University provided with the TEM measurement and ^{1}H NMR, respectively, and we also thank Dr Y. Wang from Instrument Analysis Center of Xi'an Jiaotong University for her assistance with PLQY measurements.

Notes and references

1 Q. Akkerman, G. Raino, M. Kovalenko and L. Manna, *Nat. Mater.*, 2018, **17**, 394–405.
2 K. Shen, X. Li, H. Xu, M. Wang, X. Dai, J. Guo, T. Zhang, S. Li, G. Zou, K. Choy, I. Parkin, Z. Guo, H. Liu and J. Wu, *J. Mater. Chem. A*, 2019, **7**, 6134–6142.
3 L. Schmidt, A. Pertegas, S. Carrero, O. Malinkiewicz, S. Agouram, G. Espallargas, H. Bolink, R. Galian and J. Perez-Prieto, *J. Am. Chem. Soc.*, 2014, **136**, 850–853.
4 J. Xi, K. Xi, A. Sadhanala, K. Zhang, G. Li, H. Dong, T. Lei, F. Yuan, C. Ran, B. Jiao, P. Coxon, C. Harris, X. Hou, R. Kumar and Z. Wu, *Nano Energy*, 2019, **56**, 741–750.
5 L. Wang, L. Meng, L. Chen, S. Huang, X. Wu, G. Dai, L. Deng, J. Han, B. Zou, C. Zhang and H. Zhong, *J. Phys. Chem. Lett.*, 2019, **10**, 3248–3253.
6 L. Protesescu, S. Yakunin, M. Bodnarchuk, F. Krieg, R. Caputo, C. Hendon, R. Yang, A. Walsh and M. Kovalenko, *Nano Lett.*, 2015, **15**, 3692–3696.
7 C. Wang, S. Lin, A. Tang, B. Singh, H. Tong, C. Chen, Y. Lee, T. Tsai and R. Liu, *Angew. Chem., Int. Ed.*, 2016, **55**, 7924–7929.
8 M. Yang, Y. Xu, J. Liao, X. Wang, H. Chen and D. Kuang, *J. Mater. Chem. A*, 2019, **7**, 5409–5415.
9 Y. Wei, Z. Cheng and J. Lin, *Chem. Soc. Rev.*, 2019, **48**, 310–350.
10 O. Akkerman, M. Gandini, F. Stasio, P. Rastogi, F. Palazon, G. Bertoni, J. Ball, M. Prato, A. Petrozza and L. Manna, *Nat. Energy*, 2016, **2**, 16194.
11 F. Ye, H. Zhang, W. Li, Y. Yan, J. Cai, R. Gurney, A. Pearson, D. Liu and T. Wang, *Small Methods*, 2019, **3**, 1800489.
12 Y. Zhang, R. Sun, X. Ou, K. Fu, Q. Chen, Y. Ding, L. Xu, L. Liu, Y. Han, A. Malko, X. Liu, H. Yang, O. Bakr, H. Liu and O. Mohammed, *ACS Nano*, 2019, **13**, 2520–2525.
13 J. Roo, M. Ibanez, P. Geiregat, G. Nedelcu, W. Walravens, J. Maes, J. Martins, I. Driessche, M. Kovalenko and Z. Hens, *ACS Nano*, 2016, **10**, 2071–2081.
14 D. Yang, X. Li, W. Zhou, S. Zhang, C. Meng, Y. Wu, Y. Wang and H. Zeng, *Adv. Mater.*, 2019, 1900767.
15 S. Smock, T. Williams and R. Brutchey, *Angew. Chem., Int. Ed.*, 2018, **57**, 11711–11715.
16 H. Dong, J. Xi, L. Zuo, J. Li, Y. Yang, D. Wang, Y. Yu, L. Ma, C. Ran, W. Gao, B. Jiao, J. Xu, T. Lei, F. Wei, F. Yuan, L. Zhang, Y. Shi, X. Hou and Z. Wu, *Adv. Funct. Mater.*, 2019, **29**, 1808119.
17 M. Boles, D. Ling and T. Hyeon, *Nat. Mater.*, 2016, **15**, 141–153.
18 A. Swarnkar, R. Chulliyil, V. Ravi, M. Irfanullah, A. Chowdhury and A. Nag, *Angew. Chem., Int. Ed.*, 2015, **54**, 15424–15428.
19 J. Dai, J. Xi, L. Li, J. Zhao, Y. Shi, W. Zhang, C. Ran, B. Jiao, X. Hou, X. Duan and Z. Wu, *Angew. Chem., Int. Ed.*, 2018, **57**, 5754–5758.
20 J. Kang and L. Wang, *J. Phys. Chem. Lett.*, 2017, **8**, 489–493.
21 F. Stasio, S. Christodoulou, N. Huo and G. Konstantatos, *Chem. Mater.*, 2017, **29**, 7663–7667.
22 B. Bohn, Y. Tong, M. Gramlich, M. Lai, M. Döblinger, K. Wang, R. Hoye, P. Buschbaum, S. Stranks, A. Urban, L. Polavarapu and J. Feldmann, *Nano Lett.*, 2018, **18**, 5231–5238.
23 F. Li, Y. Liu, H. Wang, Q. Zhan, Q. Liu and Z. Xia, *Chem. Mater.*, 2018, **30**, 8546–8554.
24 J. Woo, Y. Kim, J. Bae, T. Kim, J. Kim, D. Lee and S. Jeong, *Chem. Mater.*, 2017, **29**, 7088–7092.
25 G. Li, J. Huang, H. Zhu, Y. Li, J. Tang and Y. Jiang, *Chem. Mater.*, 2018, **30**, 6099–6107.
26 H. Li, Y. Qian, X. Xing, J. Zhu, X. Huang, Q. Jing, W. Zhang, C. Zhang and Z. Lu, *J. Phys. Chem. C*, 2018, **122**, 12994–13000.
27 B. Koscher, J. Swabeck, N. Bronstein and A. Alivisatos, *J. Am. Chem. Soc.*, 2017, **139**, 6566–6569.
28 T. Ahmed, S. Seth and A. Samanta, *Chem. Mater.*, 2018, **30**, 3633–3637.
29 D. Nenon, K. Pressler, J. Kang, B. Koscher, J. Olshansky, W. Osowiecki, M. Koc, L. Wang and A. Alivisatos, *J. Am. Chem. Soc.*, 2018, **140**, 17760–17772.
30 J. Pan, Y. Shang, J. Yin, M. Bastiani, W. Peng, I. Dursun, L. Sinatra, A. El-Zohry, M. Hedhili, A. Emwas, O. Mohammed, Z. Ning and O. Bakr, *J. Am. Chem. Soc.*, 2018, **140**, 562–565.

31 Z. Li, L. Kong, S. Huang and L. Li, *Angew. Chem., Int. Ed.*, 2017, **56**, 8134–8138.
32 J. Pan, S. Sarmah, B. Murali, I. Dursun, W. Peng, M. Parida, J. Liu, L. Sinatra, N. Alyami, C. Zhao, E. Alarousu, T. Ng, B. Ooi, O. Bakr and O. Mohammed, *J. Phys. Chem. Lett.*, 2015, **6**, 5027–5033.
33 D. Meggiolaro and F. Angelis, *ACS Energy Lett.*, 2018, **3**, 2206–2222.
34 G. Ahmed, J. El-Demellawi, J. Yin, J. Pan, D. Velusamy, M. Hedhili, E. Alarousu, O. Bakr, H. Alshareef and O. Mohammed, *ACS Energy Lett.*, 2018, **3**, 2301–2307.
35 W. Xu, Q. Hu, S. Bai, C. Bao, Y. Miao, Z. Yuan, T. Borzda, A. J. Barker, E. Tyukalova, Z. Hu, M. Kawecki, H. Wang, Z. Yan, X. Liu, X. Shi, K. Uvda, M. Fahlman, W. Zhang, M. Duchamp, J. Liu, A. Petrozza, J. Wang, L. Liu, W. Huang and F. Gao, *Nat. Photonics*, 2019, **13**, 418–424.
36 C. Bi, S. Kershaw, A. Rogach and J. Tian, *Adv. Funct. Mater.*, 2019, **29**, 1902446.
37 J. Song, T. Fang, J. Li, L. Xu, F. Zhang, B. Han, Q. Shan and H. Zeng, *Adv. Mater.*, 2018, 1805409.
38 J. Song, J. Li, L. Xu, J. Li, F. Zhang, B. Han, Q. Shan and H. Zeng, *Adv. Mater.*, 2018, **30**, 1800764.
39 Y. Song, J. Yoo, E. Ji, C. Lee, G. Han, H. Jung and D. Yoon, *Chem. Eng. J.*, 2016, **306**, 791–795.
40 E. Jang, S. Jun, H. Jang, J. Lim, B. Kim and Y. Kim, *Adv. Mater.*, 2010, **22**, 3076–3080.
41 M. Mikami, S. Shimooka, K. Uheda, H. Imura and N. Kijima, *Key Eng. Mater.*, 2008, **403**, 11–14.
42 R. Xie, N. Hirosaki, N. Kimura, K. Sakuma and M. Mitomo, *Appl. Phys. Lett.*, 2007, **90**, 191101.

